

Notched Beam Specimen Flexure through Modified Crack Propagation Finite Element Model

M. Smetana & L. Khazanovich

Department of Civil and Environmental Engineering, University of Pittsburgh, Pittsburgh, Pennsylvania, United States of America

S. Sen

Department of Civil Engineering, Indian Institute of Technology, Gandhinagar, Gujarat, India

ABSTRACT: Cohesive Zone Models (CZMs) are valuable tools in finite element modeling of crack propagation in concrete structures, including concrete pavements. A recent 2D crack element, developed by Sen & Khazanovich (2021), provides a simplified and computationally efficient approach for modeling crack behavior, including the simulation of concrete's flexural performance. While effective, the model does not currently account for notched beam geometries, which are essential for comparisons with experimental data. Additionally, the existing solution procedure involves matrix inversions for all elements, including those with unchanged stiffness, leading to computational inefficiencies. This paper extends the crack element model by incorporating notched beam geometry and introducing a modified solution procedure to reduce computational demands. Results show that increasing notch depth decreases tensile strength, while sensitivity to the kink-point ratio in the bilinear traction law remains limited. The proposed modifications significantly enhance computational performance and accuracy, laying the groundwork for future calibration and validation against experimental data.

1 INTRODUCTION

In rigid pavements, the tensile failure of concrete is intentionally utilized as a design mechanism due to the relatively large tensile stresses caused by heavy traffic loading conditions and thermal gradients. Since the tensile strength of concrete is difficult to measure directly, indirect methods such as the modulus of rupture have been adopted (Wittman, 2005).

The modulus of rupture (f_r), or flexural strength, is a measure of the maximum amount of stress that a material can withstand before breaking or failing under a bending load. Higher f_r values correspond to the materials' ability to have a greater resistance to cyclic loading (e.g., traffic loads or freeze-thaw cycles). While this property characterizes the apparent flexural strength of concrete, it is evident that it is also dependent on related fracture mechanisms such as the size effect or the overall fracture energy required to initiate crack propagation (Bažant and Li, 1995).

Due to the quasi-brittle nature of concrete, linear elastic fracture mechanics (LEFM) only provide a limited accuracy in numerical analyses. Quasi-brittle materials tend to exhibit a large, nonlinear, fracture process zone (FPZ) in front of the crack tip, which other models like Cohesive Zone Models (CZMs) seek to address (Hillerborg et al., 1976). Essentially, a CZM characterizes the relationship between traction and separation at the crack tip; Therefore, traction laws can be defined to represent these processes at crack interface.

Roesler et al. (2007) implemented a bilinear traction law for CZM analysis of concrete flexural tests. In their study, cohesive elements were placed at the boundary of a crack at the center of a beam model, closely resembling testing conditions. However, finite element models like this typically require extremely fine meshes near the crack. More recently, Sen & Khazanovich (2021) developed a simplistic 2D finite element model, referred to as the “self-contained” crack element, to reduce mesh complexity and improve computational efficiency.

This model has effectively simulated crack propagation in beams in both flexural and tension scenarios, showing relationships between f_r and CZM parameters. However, the model has not yet been adapted to include a notch in the beam geometry. The inclusion of a notch is particularly important for facilitating mode I (pure bending) fracture, ensuring that a crack propagates at midspan during three- or four-point bending laboratory tests (Yin et al., 2019).

This paper proposes a modified version of the self-contained crack element model. The inclusion of a notch enables future comparisons with experimental data. Additionally, the modified model reduces the number of matrix inversion operations, further enhancing computational speed. These changes aim to improve the model's accuracy and provide more refined estimates of values such as the modulus of rupture for use in rigid pavement design.

2 ELEMENT MODELING

The model consists of an intermediate self-contained crack element surrounded by Euler beam elements, as shown in Figure 1. Each connecting node allows for rotation and translation in the x and y direction. The two nodes connected to the boundary of the crack element undergo iterative displacements to simulate the loading conditions.

A beam in this analysis is comprised of a length (L) in the y direction, height (h) in the x direction, and a unit thickness (b) for simplified 2D modeling. The $L/3$ dimensions serve as an example of four-point bending conditions.

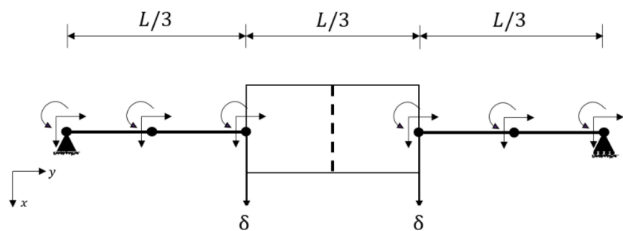


Figure 1. Self-contained crack element model

2.1 Crack element

The crack element is defined by a combination of cohesive Park–Paulino–Roesler (PPR) elements (Park et al., 2009) with pre-meshed bulk elements, as shown in Figure 2. There are N_x bulk elements in the x direction and $2N_y$ in the y direction. The multiplication by two in the y direction accounts for model symmetry about the center of the beam, only requiring user input for half of the number of elements. There must be an additional element along the length of the beam to include the zero-width cohesive elements, resulting in a total number of $N_x \times (2N_y + 1)$ elements.

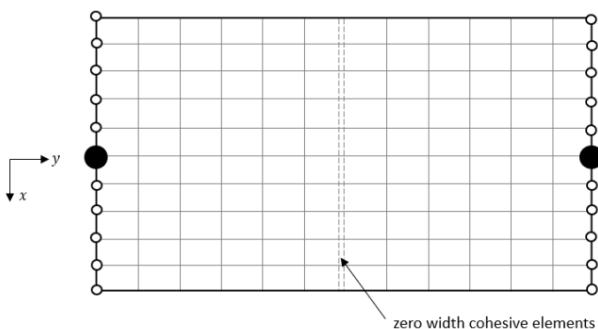


Figure 2. Bulk and zero-width cohesive elements within crack element

2.1.1 Bulk elements

The stiffness matrix of the bulk elements are based on bilinear, quadrilateral elements, described by Young's modulus (E), Poisson's ratio (ν), and two degrees of freedom (DOF) at each node for translations. Since this is a 2D finite element analysis, it is assumed that the thickness of the beam, b , is much

smaller than the length and height; thus, a plane stress state is used for stiffness matrix evaluation.

2.1.2 Cohesive elements

A bilinear traction separation law (Figure 3) characterizes crack propagation in the cohesive elements. Other CZM models can be implemented in future analyses, if necessary. This bilinear law is a function of crack opening width (w), stress (σ), total fracture energy (ϕ), and kink-point ratio (ψ) – which relates to the transition between initial linear elastic behavior and subsequent softening behavior for materials under tension (Roesler et al., 2007). This ratio is critical for understanding how cracks initiate and propagate, as it helps define the tensile strength (f'_t) and crack opening metrics of the material (Tompkins et al., 2015).

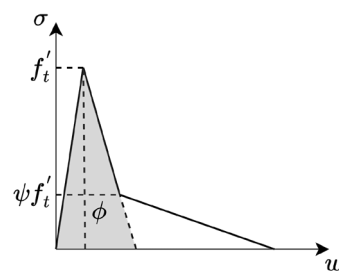


Figure 3. Bilinear softening curve adapted from Roesler et al. (2007)

2.2 Euler beam elements and connections

Each beam element is then characterized by their geometry and Young's Modulus (E). The development of a transverse crack creates an additional moment, coupling with axial displacements (Rice & Levy, 1972), leading to three DOFs (axial, transverse, and rotational) instead of the typical two in conventional beam elements (only axial and transverse). Individual stiffness matrices are evaluated as a combination of Euler-Bernoulli beam theory and rod theory (Zienkiewicz et al., 2000).

Part of the modeling process involves linking the crack element to the neighboring rod elements, which is further described in the original paper (Sen & Khanzavich, 2021).

2.3 Notched beam adaptation

To implement a notched beam into the model, a new user input for notch ratio (a/h) is required. In this case a is the depth of the notch and h is the height of the beam (Figure 4), as previously mentioned.

During the iterative solution procedure, the cohesive stress between nodes connecting the zero-width element to the bulk elements is set to zero. This allows the solver to treat these elements as already separated and to focus on the remaining, unsevered

elements for stress development. By fixing one support condition and allowing the other support to move freely in the y -direction, this resembles similar conditions to experimental testing.

This four point bending configuration ensures that the beam will be loaded in a purely bending fashion and eliminate the effect of any shear forces developing within the crack, which is commonly adjusted in the experimental post-processing of three point notched beam fracture tests.

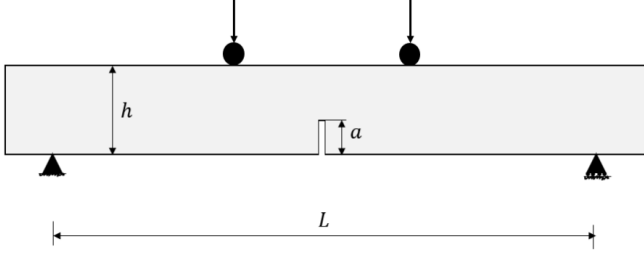


Figure 4. Typical notched beam four-point bending test configuration

3 MODIFIED SOLUTION PROCEDURE

This self-contained crack element model significantly reduces the computational complexity required to run analyses – relative to other finite analyses that require a much finer mesh around the crack zone. An accurate analysis with the model proposed in this study requires approximately 10 elements in both the x and y direction of the crack element, which is the only part of the model that has any bulk elements.

Sen & Khazanovich (2021) proposed the following five-step procedure for modeling crack propagation:

Step 1: Evaluation of Element Properties: The stiffness matrix and force vector for beam elements and the crack element are computed, incorporating bulk and cohesive components. Displacements from the previous time increment are used for cohesive elements.

Step 2: Reduction of Crack Element: The stiffness matrix and force vector of the crack element are reduced to boundary nodes using static condensation. The algorithm involves partitioning the stiffness matrix of the crack element, K_{cr} , as well as the corresponding force and displacement vectors, f_{cr} and u_{cr} respectively, into boundary (subscript b) and interior (subscript i) DOFs to obtain the relationship:

$$\begin{bmatrix} K_{bb} & K_{bi} \\ K_{ib} & K_{ii} \end{bmatrix} \begin{pmatrix} u_b \\ u_i \end{pmatrix} = \begin{pmatrix} f_b \\ f_i \end{pmatrix} \quad (1)$$

Then, the condensed stiffness matrix and force vector corresponding to the boundary nodes, K_{bb}^* and f_b^* :

$$K_{bb}^* = k_{bb} - K_{bi}K_{ii}^{-1}K_{ib}; f_b^* = f_b - K_{bi}K_{ii}f_i \quad (2)$$

Step 3. Integration into Beam Model: The reduced crack element is connected to adjacent beam elements.

Step 4. Assembly and Solution: All element matrices and vectors are assembled, boundary conditions are applied, and the system is solved using an FE solver.

Step 5. Displacement Reconstruction: Node displacements (u_b and u_i) are reconstructed for use in the next iteration, completing the time-step loop.

This approach was adapted in this study, wherein Step 2 was significantly modified. The drawback of the procedure described above is the requirement to inverse the stiffness matrix K_{ii} at every time increment. However, the majority of the elements forming this portion of the structure are linear elastic, i.e. not changing from one time-step to another, while stiffnesses of only a small number of cohesive elements have to be adjusted. To address this limitation, the nodes of the crack element were partitioned into three groups: boundary (subscript b), cohesive (subscript c) and interior (subscript e), i.e. not belonging either to the boundary or cohesive elements leading to the following relationship:

$$\begin{bmatrix} K_{bb} & K_{be} & K_{bc} \\ K_{eb} & K_{ee} & K_{ec} \\ K_{cb} & K_{ce} & K_{cc} \end{bmatrix} \begin{pmatrix} u_b \\ u_e \\ u_c \end{pmatrix} = \begin{pmatrix} f_b \\ f_e \\ f_c \end{pmatrix} \quad (3)$$

Then, the condensed stiffness matrix and force vector corresponding to the boundary nodes, K_{bb}^* and f_b^* :

$$K_{bb}^* = K_{bb} - K_{be}K_{ee}^{-1}K_{eb} - K_{be}K_{ee}^{-1}K_{ec}(K_{cc} - K_{ce}K_{ee}^{-1}K_{ec})^{-1}K_{ce}K_{ee}^{-1}K_{eb} \quad (4)$$

$$f_b^* = f_b + K_{be}K_{ee}^{-1}K_{ec}(K_{cc} - K_{ce}K_{ee}^{-1}K_{ec})^{-1}(f_c - K_{ce}K_{ee}^{-1}f_e) \quad (5)$$

The advantage of this approach is that only matrix K_{cc} changes from one time increment to another. All other matrixes should be computed only in the first time increment. Computation of the condensed stiffness matrix for other steps requires only inversion of the matrix $(K_{cc} - K_{ce}K_{ee}^{-1}K_{ec})$ and its multiplication to the pre-computed matrixes. This significantly improves computational efficiency of the process.

4 EFFECT OF NOTCH ON FLEXURAL STRENGTH

From a single crack element simulation, the flexural strength (f_r) is computed with the resulting peak load P , as defined in the following equation:

$$f_r = \frac{PL}{bh^2} \quad (6)$$

To investigate the effect of notch depth on flexural strength, a factorial analysis of the inputs described in Table 1 was conducted, resulting in over 3,000 cases.

A notch ratio of zero is not considered, as it corresponds to the original model solution. The notch ratio was incremented by 0.1, ranging from 0.1 to 0.5, where 0.5 represents a notch depth equal to half the beam height.

Material properties such as E , ϕ , and ψ , were selected within typical ranges for concrete. The beam geometry was fixed to a height of 150 mm and an overall span length of 450 mm to reflect standard laboratory flexural tests. For the 2D plane-stress finite element analysis, a unit width of 1 mm was used. A tensile strength (f_t') of 3.4 N/mm² was assumed and applied to produce nondimensional results.

Table 1. Ranges of variables for factorial

Variable	Desc.	Unit	Range
a/h	notch ratio	~	0.1-0.5
E	elastic modulus	N/mm ²	31,000-50,000
ϕ	total fracture energy	N/mm	0.100-0.250
ψ	kink-point ratio	~	0.200-0.500

Figure 5 presents the results of the factorial analysis for flexural strength versus Hillerborg's characteristic length (I_{ch}), used to characterize fracture based on the associated inputs and scaled to the input tensile strength (Hillerborg et al., 1976):

$$\frac{I_{ch}}{h} = \frac{\phi E}{h f_t'^2} \quad (7)$$

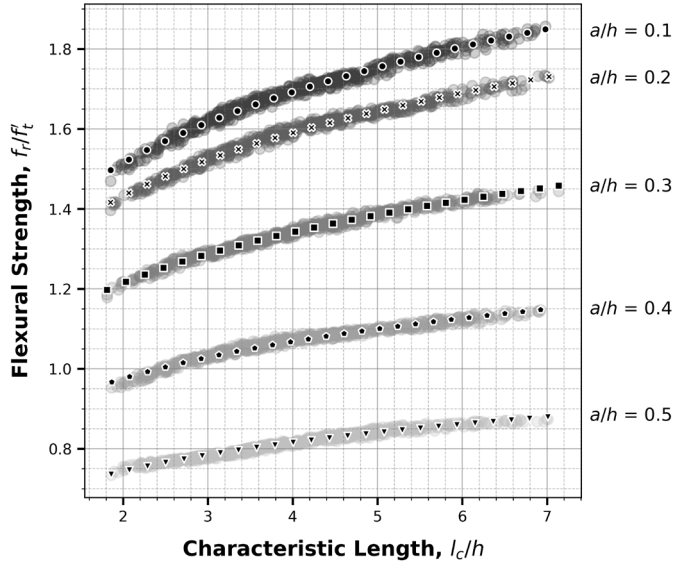


Figure 5. Nondimensional flexural strength versus characteristic length

This factorial reveals a minimum flexural strength of 2.50 N/mm² when the notch ratio is 0.5 with a characteristic length of 1.86 ($\phi = 0.102$ N/mm, $E = 31,000$ N/mm²). A maximum flexural strength of 6.31 N/mm² is observed when the notch ratio is 0.1 with a characteristic length of 6.98 ($\phi = 0.248$ N/mm, $E = 48,800$ N/mm²).

5 CONCLUSION

This paper presents an adaptation of the self-contained crack element developed by Sen & Khazanovich (2017), incorporating the notch ratio as a user input and modifying the solution procedure to enhance computational efficiency. The results demonstrate the expected influence of notch depth on the flexural strength. Furthermore, the analysis reveals that the model exhibits limited sensitivity to the kink-point ratio, ψ , suggesting that fracture in notched specimens is primarily governed by fracture energy in the bilinear CZM formulation and the four-point bending configuration.

The proposed approach enables rapid simulation, providing an opportunity to compare the results with experimental data from four-point bending tests for further calibration and validation of the model. However, the model still requires the total fracture energy (ϕ) as an input, necessitating nontrivial experimental procedures involving precise monitoring of crack mouth opening displacement (CMOD). In the future, this demanding testing may be replaced by a simplified method to measure the flexural strength, provided a reliable correlation between fracture and other engineering properties is established.

6 REFERENCES

- Bažant Z.P. & Li, Z. 1995. Modulus of Rupture: Size Effect due to Fracture Initiation in the Boundary Layer. *Journal of Structural Engineering* 121: 739-746.
- Hillerborg, A., Modeer, M. & Peterson, P-E. 1976. Analysis of crack formation and crack growth in concrete by means of fracture mechanics and finite elements. *Cement and Concrete Research* 6: 773-782.
- Park, K., Paulino, G. H., & Roesler, J. R. (2009). A unified potential-based cohesive model of mixed-mode fracture. *Journal of the Mechanics and Physics of Solids* 57(6): 891-908.
- Rice J.R. & Levy, N. 1972. The part-through surface crack in an elastic plane. *Journal of Applied Mechanics* 39(1): 185-194
- Roesler, J., Paulino, G. H., Park, K. & Gaedicke, C. 2007. Concrete fracture prediction using bilinear softening. *Cement & Concrete Composites* 29: 300-312.
- Sen, S. & Khazanovich, L. 2021. A self-contained element for modeling crack propagation in beams. *Engineering Fracture Mechanics* 242: 107460.
- Tompkins, D., Khazanovich, L. & Bolander, J.E. 2015. Lattice modeling of fracture in composite concrete pavements and overlays. *International Journal of Pavement Engineering* 16(1): 56-68.
- Wittman, F.H. 2005. Modulus of Rupture, Tensile Strength, and Fracture Energy – An Application of Non-linear Fracture Mechanics. *Restoration of Buildings and Monuments* 11(3): 141-150.
- Yin, Y., Qiao, Y. & Hu, S. 2019. Four-point bending tests for the fracture properties of concrete. *Engineering Fracture Mechanics* 211: 371-381.
- Zienkiewicz, O., Taylor, R. L. & Taylor R. L. 2000. The finite element method: solid mechanics. *Butterworth-Heinemann*.